Human Molecular Genetics, 2019, Vol. 28, No. 16 2775–2784

doi: 10.1093/hmg/ddz106
Advance Access Publication Date: 20 May 2019
General Article

GENERAL ARTICLE

A null allele of *Dnaaf2* displays embryonic lethality and mimics human ciliary dyskinesia

Agnes Cheong, Rinat Degani, Kimberly D. Tremblay and Jesse Mager*

Department of Veterinary and Animal Sciences, University of Massachusetts, Amherst, MA 01003, USA

*To whom correspondence should be addressed at: Department of Veterinary and Animal Sciences, University of Massachusetts, 661 North Pleasant Street, Amherst, Massachusetts 01003, USA. Tel: +1 4135457368; Fax: +1 4135456326; Email: jmager@vasci.umass.edu

Abstract

The dynein axonemal assembly factor (Dnaaf) protein family is involved in preassembly and stability of dynein arms before they are transported into the cilia. In humans, mutations in *DNAAF* genes lead to several diseases related to cilia defects such as primary ciliary dyskinesia (PCD; OMIM: 612518). Patients with PCD experience malfunctions in cilia motility, which can result in inflammation and infection of the respiratory tract among other defects. Previous studies have identified that a mutation in *DNAAF2* results in PCD and that 40% of these patients also experience laterality defects. In an outbred genetic background, *Dnaaf2* homozygotes die after birth and have left/right defects among other phenotypes. Here we characterize a novel null allele of *Dnaaf2* obtained from the International Mouse Phenotyping Consortium. Our data indicate that on a defined C57bl/6NJ genetic background, homozygous *Dnaaf2* mouse embryos fail to progress beyond organogenesis stages with many abnormalities including left–right patterning defects. These findings support studies indicating that hypomorphic mutations of human *DNAAF2* can result in ciliary dyskinesia and identify *Dnaaf2* as an essential component of cilia function *in vivo*.

Introduction

Cilia are evolutionarily conserved structures that are present in most eukaryotes (1). Although initially thought to be vestigial, it is now accepted that the majority of mammalian cell types retain a primary cilium, and many investigations have shown that cilia play important and essential roles in various signaling pathways and developmental processes (2–4). Furthermore, defects in cilia assembly greatly influence the function of cilia. There are two types of cilia; motile and primary (non-motile) cilia. Motile cilia exert mechanical force and are usually found in epithelial cells, whereas primary cilia predominantly function as a sensory organelle and are essential for initiating cellular signaling in adult tissues such as the kidney and in embryonic structures including the node (5,6).

Embryonic cells contain both motile and primary cilia (7). Primary cilia play a particularly significant role during gastrulation—the dynamic morphogenetic process that results in the organization of the three primary germ layers. At the onset of gastrulation an epithelial-to-mesenchymal transition occurs on the posterior of the embryo forming a transient structure known as the primitive streak, which extends through the midline of the embryo and contributes to the definition of the anterior–posterior axis (8). The streak extends from the proximal/posterior to the distal tip of the embryo, and the most distal/anterior tip of the primitive streak forms a unique flattened horseshoe-shaped structure, which contains organizer activity. Elegant studies have shown that this transient structure (the node) contains cilia that generate a leftward flow resulting in the first molecular break in left–right symmetry of

Received: January 31, 2019. **Revised:** April 12, 2019. **Accepted:** May 13, 2019

the developing embryo. This cilia-induced nodal flow is essential for left–right axis specification (7), and although the mechanism remains controversial, it is clear that defects in this leftward flow can result in *situs inversus* or *situs ambiguous* (9,10).

Bilateral asymmetry requires specific spatiotemporal gene expression (11). In the mouse embryo, the leftward flow generated at the node results in asymmetric *Nodal* expression, which produces asymmetric gene expression in the lateral plate mesoderm (12,13). *Nodal* promotes expression of *Pitx2*, a gene that is normally expressed only on the left-side lateral plate mesoderm (in response to the presence of *Nodal* on the left side of the node) (14). *Sonic hedgehog* (*Shh*) has been shown to be upstream of *Nodal*, and in *Shh* null mouse embryos the left–right axis is compromised with a variety of laterality defects including misexpression of *Nodal*, *Pitx2*, *Lefty1* and other left–right specific expression (14). It has been hypothesized that the asymmetric gene expression is generated by both motile and primary cilia at the node (14). This idea is supported by studies of mutant mice with immotile cilia as well as mutants without any nodal cilia (15,16). In both cases, genes that are typically expressed on either the left or right are found to be bilaterally or abnormally expressed in the mutant embryos.

The dynein axonemal assembly factor (Dnaaf) protein family is involved in the preassembly and stability of dynein arms before they are transported into the cilia (17–21). In humans, mutations in *DNAAF* genes lead to several diseases related to cilia defects such as primary ciliary dyskinesia (PCD) (19,21–23). Patients with PCD experience malfunctions in cilia motility, which can result in inflammation and infection in the respiratory tract among other defects (24). Previous studies have identified that a mutation in *DNAAF2* results in PCD and that 40% of these patients also experience laterality defects (17,21,25). Mammalian cells lacking *Dnaaf2* have defects in both the outer and inner dynein arms, resulting in a loss of cilia motility (17,18). Malfunction of cilia during embryonic development can also result in laterality defects and left–right axis abnormalities (7).

As mentioned above, human *DNAAF2* can result in ciliary dyskinesia and laterality defects. However, little is known about the role of *Dnaaf2* during embryogenesis. The Knockout Mouse Project (KOMP) is part of a global initiative to generate a null mutation in every gene within the mouse genome. The goal of the project is to elucidate the function of every gene and evaluate potential involvement in human health and disease. While the major focus has been on identifying genetic mutations resulting in adult phenotypes related to human disease, a large percentage of knockout (KO) alleles result in homozygous embryonic lethal phenotypes (26,27). Here we report that in the absence of *Dnaaf2*, embryos fail to develop beyond early organogenesis, with abnormalities including left–right patterning defects. Consistent with finding in other species, our data suggest that *Dnaaf2* does not interact directly with left–right signaling pathways but is required for proper cilia function and nodal flow.

Results

Expression of *Dnaaf* genes

We first determined the expression of *Dnaaf2* in various adult mouse tissues. Since *Dnaaf2* is associated with proper cilia function, it is not surprising that the gene is expressed in multiciliated tissues including brain, kidney, liver, lung, ovary, oviduct, spleen and testis (Fig. 1A). This result also correlates well with a previous study of *Dnaaf2* in mouse tissues (19). We also examined the expression of the other *Dnaaf* family members in adult mouse tissues. Past work has identified *DNAAF1* to be crucial for neural tube development in humans (28), where its main role is to provide stability for the ciliary structure. *DNAAF2*, *DNAAF3* and *DNAAF4* (18–20,29) are associated with laterality and cilia motility in humans, and *Dnaaf2* was shown to interact with *Dnaaf4* in mouse respiratory epithelial cells (20). *DNAAF5* is essential for transporting ciliary machinery to the motile axoneme (30). Unlike other DNAAF members, DNAAF5 does not interact with the chaperone proteins and has been found to colocalize with DNAAF2 and other proteins to form the early preassembly complex (29). Consistent with the role of the *Dnaaf* family, these genes are all expressed in oviduct and testis (Fig. 1A) where cilia play an essential role in tubal transport *in vivo* and tubule formation and cellular signaling in testicular somatic cells *in vitro* (31–33). Specifically, *Dnaaf1* is expressed at high level in brain, ovary, oviduct and testis but expressed at low level in heart, kidney, liver, lung and spleen; *Dnaaf2*, *Dnaaf4* and *Dnaaf5* are expressed in all tissues examined (brain, heart, kidney, liver, lung, ovary, oviduct, spleen and testis); and *Dnaaf3* expression is largely restricted to lung, ovary, oviduct and testis (Fig. 1A). Previous studies have shown that *DNAAF4* and *DNAAF5* physically interact with *DNAAF2* (20,29), so it is perhaps not surprising that we observe similar expression patterns for these genes.

It is currently unknown when or where *Dnaaf* family members are expressed during embryonic development. Therefore, we assessed *Dnaaf* family gene expression in wild-type embryos at specific developmental stages in mouse embryos: blastocyst (E3.5), gastrulation (E6.5–8.5) and organogenesis (E9.5) stage embryos (Fig. 1B).

Dnaaf2 is the only family member expressed in the blastocysts during preimplantation. *Dnaaf4* and *Dnaaf5* have similar temporal expression beginning at E6.5. Conversely, *Dnaaf1* and *Dnaaf3* are not expressed at appreciable levels during any embryonic stage tested (Fig. 1B). It is worth noting that besides *Dnnaf2*, *Dnaaf4* and *Dnaaf5* are expressed robustly beginning at the onset of gastrulation. The expression pattern of *Dnaaf2*, *Dnaaf4* and *Dnaaf5* overlaps at the onset of gastrulation suggesting the importance of these *Dnaaf* members in promoting proper functional cilia at this specific stage of development. To evaluate spatiotemporal and tissue-specific expression, we performed whole-mount *in situ* hybridization (ISH) with two distinct antisense probes using intron-spanning primers designed against *Dnaaf2* (only one shown). *Dnaaf2* mRNA is present specifically in the epiblast at E6.5 and in all newly specified embryonic lineages at E7.5 but is conspicuously absent from all extraembryonic lineages, even those that are primitive streak derived including the allantois and yolk sac mesoderm (Fig. 1C and D). Importantly, *Dnaaf2* is expressed in the embryonic node at E7.5. In late gastrulation and organogenesis stage embryos, *Dnaaf2* expression becomes further restricted to the lateral plate mesoderm, the neural tube, gut tube and first branchial arch (Fig. 1E and F). As expected, *Dnaaf2* signal was completely absent in *Dnaaf2*$^{-/-}$ embryos (Fig. 1G) confirming the specificity of the ISH expression patterns observed.

Dnaaf2 function is essential for normal embryo development

To determine the role of *Dnaaf2*, we obtained a *Dnaaf2* KO allele generated at the Jackson Laboratories as part of the KOMP (26). This mutation was produced by replacing the majority of the endogenous locus with a *lacZ* reporter gene, resulting in deletion

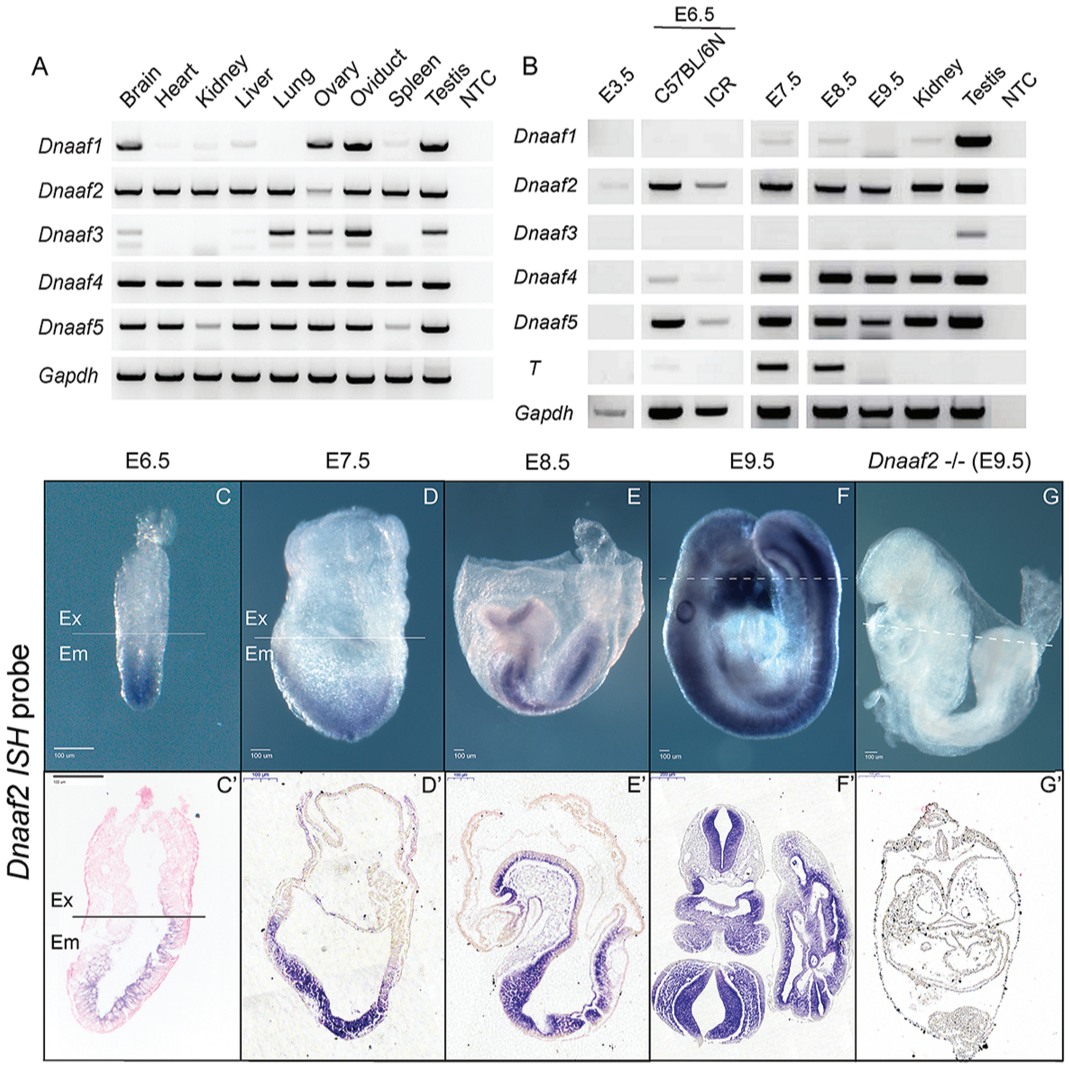

Figure 1. *Dnaaf2* is expressed in various adult mouse tissues and across different stages of mouse embryos. (**A** and **B**) RNA was freshly extracted from adult mouse tissues, and cDNA was synthesized for reverse transcription polymerase chain reaction (RT-PCR) analysis. *T* (brachyury) and *Gapdh* were used for indicating embryonic stages and loading control. (A) *Dnaaf2* is expressed in multiple ciliated adult mouse tissues. (**C–G**) To more closely examine *Dnaaf2* expression during development, embryos were collected at the indicated embryonic day (E), and whole-mount ISH was performed using *Dnaaf2* antisense probe that is generated from intron-spanning primers that are complementary to the protein-coding regions of exon 1 and exon 3 (Fig. 3C). During embryo development, *Dnaaf2* is expressed throughout the embryonic lineage beginning at E6.5 and develops tissue specificity at organogenesis (C′–F′). Sagittal section, C′, D′ and E′; transverse section, F′ and G′; –/– denotes *Dnaaf2* mutant embryo; dotted line denotes the transverse section shown in C′, F′ and G′; Ex denotes extraembryonic portion; and Em denotes embryonic portion.

of 8457 bases (*Dnaaf2*$^{tm1.1(KOMP)Vlcg}$). A previous large-scale screen of viability in newly generated alleles identified a lack of *Dnaaf2* embryos at E15.5 (26). Surprisingly, one previous study reports that a KO of *Dnaaf2* is viable with subtle adult phenotypes (19). We believe this discrepancy is most likely explained due to genetic background and functional redundancy (discussed further below). Therefore, in order to identify the *Dnaaf2* loss-of-function phenotype in a C57bl/6NJ background, we performed heterozygous intercrosses and analyzed embryos between E6.5 and E13.5 (Fig. 2A). Genotypes of *Dnaaf2* homozygous null embryos were verified with *Dnaaf2*-specific polymerase chain reaction (PCR) primers (Fig. 2D). Comparing the morphology of *Dnaaf2*$^{-/-}$ embryos (hereafter referred to as '–/–', 'mutants' or 'mutant embryos') to wild-type and heterozygous littermates (hereafter referred to as 'control', '+/–' or '+/+' embryos), mutants show a significant developmental delay as early as gastrulation stages (E6.5–7.5, Fig. 2A). Mutants continue to develop but are grossly retarded by E8.5–9.5 and are significantly malformed and dying at later stages (E11.5 and 13.5). In addition to the developmental delay, the most obvious phenotype observed is that mutants do not initiate embryonic turning, which is essential for continued growth and development of both the placenta and embryo (Fig. 2A). At E9.5, mutant embryos have not established a vascular network in the yolk sac. This difference is most apparent when comparing the yolk sac of E11.5 mutant embryo and its littermate (Fig. 2B and C). Failure to develop the proper cardiovascular network greatly affects embryo development and the viability of the growing embryo (34). We also observe improper closure of the neural tube in the brain of most mutant embryos, most apparent in E9.5 mutant embryos (Fig. 2A). At E11.5, mutant embryos display pericardial edema, which could be a secondary defect of malformation of the cardiovascular network, which in turn may contribute to the delay in heart development (Fig. 2A). The tailbud region

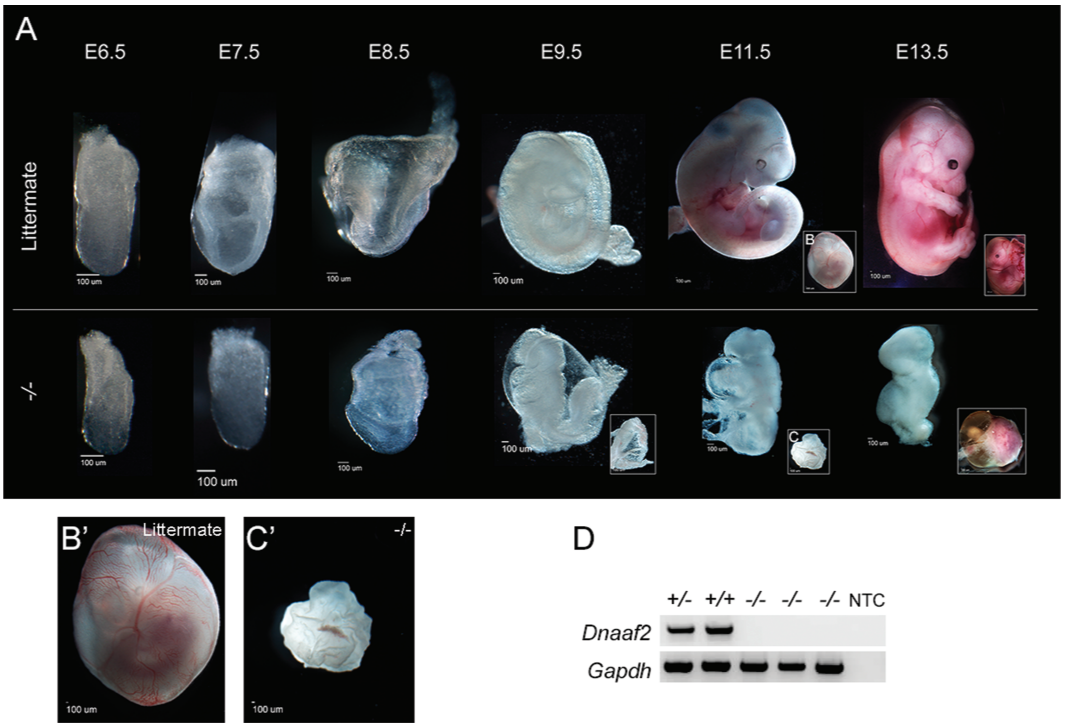

Figure 2. *Dnaaf2* $^{-/-}$ mouse embryos are delayed in development when compared to littermate. Embryos were collected at the indicated embryonic day (E). The lower panel denotes the embryo lacking both copies of the *Dnaaf2* allele, and the upper panel denotes their respective wild-type or heterozygous littermates (**A**). *Dnaaf2*$^{-/-}$ embryos are delayed in development and do not proceed through the turning of the embryos. Particularly, the E11.5 yolk sac vasculature of the *Dnaaf2*$^{-/-}$ embryo is dramatically different from its littermate (**B**, B′, **C** and C′). No *Dnaaf2* homozygous mutant embryos are recovered at time of delivery. RT-PCR result verifies that the mutant embryos do not contain the *Dnaaf2* alleles (**D**). B′ and C′ are magnified views of B and C. *Gapdh* is used as a loading control. NTC denotes no template control; +/+ denotes wild-type embryo; +/− denotes *Dnaaf2* heterozygous embryo; −/− denotes *Dnaaf2* mutant embryo. Scale bar for each image is included below each embryo.

of the mutant embryos at E11.5 also displays an abnormal cavity (Fig. 2A). This may further indicate a failure of functional connection between the embryo and the placenta. Since the placenta appears to develop normally in mutant embryos, the improper development of the vascular network in the yolk sac likely disrupts umbilical cord development (35) and hence contributes to the overall delay in development (Fig. 2A).

Dnaaf2 is required for proper left–right patterning

Since there are known human *DNAAF2* mutations associated with laterality defects and the embryonic node is known to be essential for establishment of left–right asymmetry, we determined if and when the embryonic node forms in *Dnaaf2* mutant mouse embryos. Interestingly, although the formation and extension of the primitive streak occur at the appropriate developmental time (~E6.5) a visible node cannot be observed in E7.5 mutant embryos, a stage at which all littermates have a distinct node at the distal end of the embryo. A morphological node structure does appear in ~E8.5 mutants but is quite small in size and less well defined compared with controls of any stage (Fig. 3, compare A to B).

As mentioned above, the *Dnaaf2* KO allele is generated by deleting a portion of the *Dnaaf2* genomic sequence and replacing it with a *lacZ* reporter gene (Fig. 3C). We decided to utilize the *lacZ* reporter gene and perform X-gal staining to examine the *lacZ* expression in *Dnaaf2* heterozygous embryos collected from E6.5 to E9.5 (Fig. 3D). Surprisingly, *lacZ* expression is localized at the distal tip of the embryo, precisely in the primitive node. Node-specific *lacZ* is observed at all stages of development at which the node is apparent. *LacZ* expression is absent in all other embryonic tissues and stages (Fig. 3D and E). Given the function of *Dnaaf2* and documented role in dynein arm complex assembly, *Dnaaf2* expression in the node is not unexpected. However, the *lacZ* expression pattern is strikingly different from the *Dnaaf2* mRNA expression pattern observed by multiple distinct *Dnaaf2* ISH probe, which indicates that the wide-spread embryonic expression of *Dnaaf2* mRNA is not confined to the node (Figs 1C–G and 3D and E). Since genomic sequence (both introns and exons) was removed when generating the KO allele, the most likely explanation is that these sequences contain enhancer and/or regulatory elements that normally confer wide-spread expression of *Dnaaf2*.

To evaluate organizer development in *Dnaaf2* mutant embryos, we examined the localization of *Cthrc1*, which has been shown to be expressed in the node as it is forming (36). *Cthrc1* ISH does indeed show expression in mutant embryos in a more diffuse but overall similar pattern as in control littermates (Fig. 4A–C). We further examined mutant embryos by immunofluorescent co-detection of Arl13B and brachyury (T) to determine if the mutant node contains cilia. While we do observe Arl13b/T double-positive cells indicating cilia are present in the mutant node (Fig. 4D, D′, E and E′), there are fewer Arl13b-positive cells in the mutant node, consistent with the apparent reduced node size. This observation is strikingly apparent when compared to a developmental node-stage control (wild-type E7.5 node compared to mutant E8.5 node—compare Fig. 4E, E′, F and F′).

The node contains cilia that generate a leftward flow, which gives rise to left–right asymmetry (7). Having established that

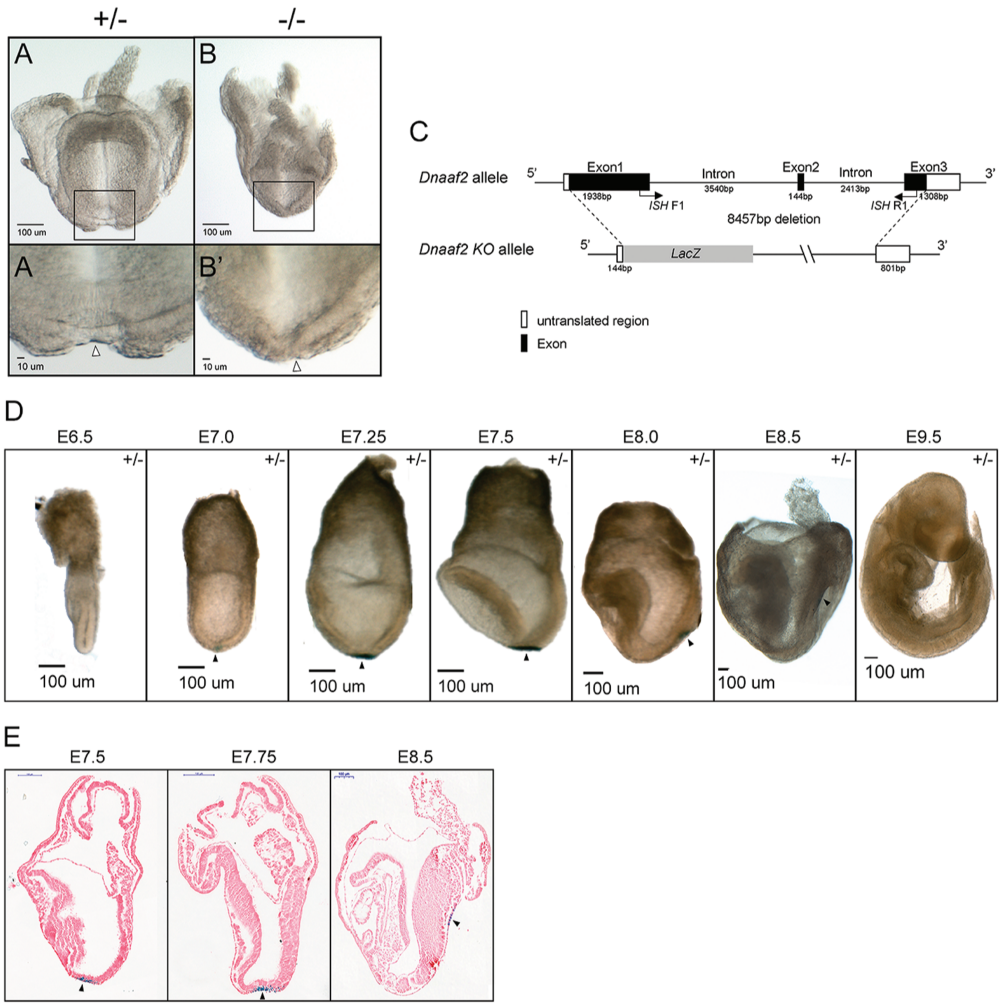

Figure 3. *Dnaaf2* $^{-/-}$ embryos have a morphologically distinct node. Embryos were collected at embryonic day (E) 8.5 and examined under a microscope for node assessment (**A** and **B**). *Dnaaf2*$^{-/-}$ embryos do have a morphologically distinct node (black hollow triangle in A′ and B′). (A′ and B′) Magnified view of node region is indicated with a black arrow. The construct of the *Dnaaf2* KO allele is generated by replacing a portion of the *Dnaaf2* genomic sequence with a cassette containing a *LacZ* reporter gene (**C**). *ISH* F1 and *ISH* R1 denote the intron-spanning primers used for the generation of *Dnaaf2* ISH probe. X-gal staining reveals *LacZ* expression precisely in the node but not in any other tissues (black triangle in **D**). *ISH* F1 and *ISH* R1 are the forward and reverse primers for *Dnaaf2* ISH probe generation. Frontal view, A and B; lateral view, D and **E**; sagittal section, E. +/− denotes *Dnaaf2* heterozygous embryo; −/− denotes *Dnaaf2* mutant embryo.

Dnaaf2 mutants do form a node (albeit delayed and small), we sought to determine if *Dnaaf2*$^{-/-}$ embryos establish left–right asymmetry. We therefore examined expression of genes with left–right specific patterns. *Pitx2* expression is normally confined to the left lateral plate mesoderm. Utilizing whole-mount ISH, we find that *Pitx2* is expressed inappropriately on the right side in 25% of mutant embryos ($n = 4$, Fig. 5A–C). Similarly, we examined *Hand1*, a gene that is expressed on the outer curvature of the left ventricle (but not the right ventricle) in control embryos. Our results show abnormal expression of *Hand1* in all mutants examined and that mutant embryos experience reverse heart looping (Fig. 5D–F). These observations indicate that *Dnaaf2* function is required for proper establishment of left–right patterning during embryogenesis possibly because of abnormal node function.

Left–right specification, including expression of *Pitx2*, is downstream of *Shh* (14). Since we observed laterality defect in *Pitx2* expression, we next determined if *Shh* is appropriately expressed in mutant embryos. Whole-mount ISH indicates that the notochord (a product of the node) displays a normal pattern of *Shh* in mutant embryos (Fig. 5G–I). These results confirm that there is normal developmental timing of *Shh* expression. Since *Pitx2* and *Hand1* are expressed at the proper developmental stage, the inappropriate lateral expression observed is not due to defects in transcriptional regulation of these loci, but rather defects in left–right pattering. This observation also suggests that *Dnaaf2* is required for the lateral specific establishment of these genes, most likely due to non- or poorly functional cilia and abrogated nodal flow in the absence of functional Dnaaf2 protein.

As mentioned earlier, we observe an obvious developmental delay (Fig. 2) and shortened posterior axis in the E9.5 *Dnaaf2*$^{-/-}$ embryos (Fig. 5G–I) when compared to the littermate or stage-matched control embryos. We speculate that the truncated phenotype observed is due to cells undergoing apoptosis at the posterior end of the embryo. As predicted, we observe many apoptotic cells in the posterior of E9.5 *Dnaaf2*$^{-/-}$ embryos, whereas the stage-matched controls have very few (Fig. 6C and D). We also find a heightened density of the terminal deoxynucleotidyl transferase dUTP nick end labeling (TUNEL)-positive cells in the neural tube of the mutant, which correlates

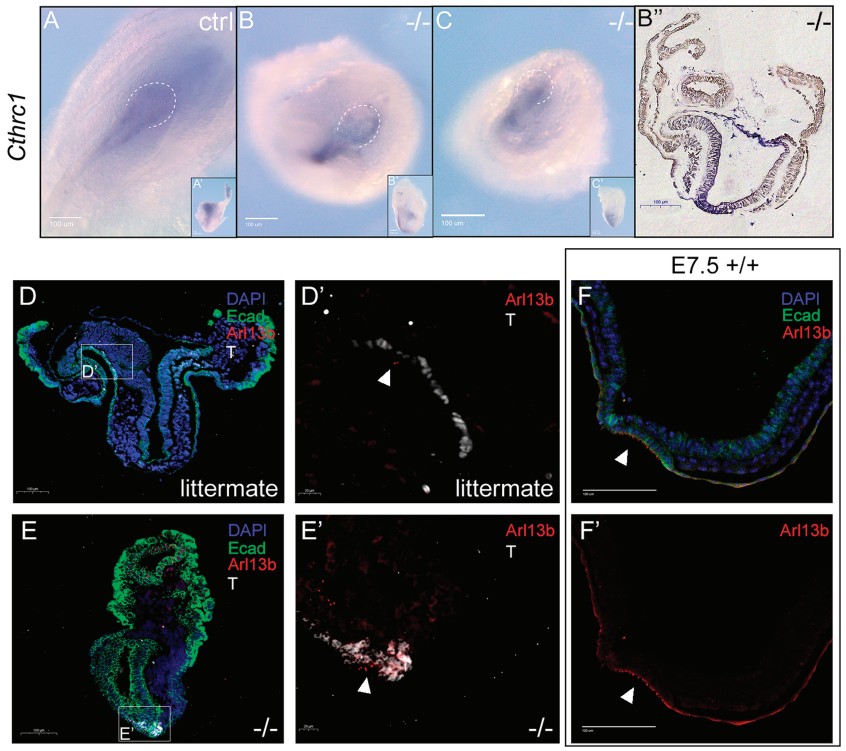

Figure 4. *Dnaaf2* $^{-/-}$ embryos contain a structure of a node and a reduction of cilia. Embryos were collected at E8.5. (**A–C**) Whole-mount ISH was performed with a *Cthrc1* antisense probe. (**D–F′**) Embryos were sagitally sectioned and immunofluorescently labeled with e-cadherin (green), T (white) and *Arl13b* (red), and the nuclei were counterstained with DAPI (blue). Similar to the littermate, *Dnaaf2*$^{-/-}$ embryos appear to have a node structure (A, B and C). The white dotted line marked the boundary of the node of the embryos. Though *Dnaaf2*$^{-/-}$ embryos were delayed in development when compared to the wild-type (E7.5 +/+) embryos (D, D′, E and E′), *Dnaaf2*$^{-/-}$ embryos appear to have a structurally normal node with cilia (B′) as expected in a E7.5 embryo (F and F′). However, there seems to be a reduction in cilia localization at the node in the *Dnaaf2*$^{-/-}$ embryos (E′ and F′). The white arrows indicate the localization of the cilia; ctrl denotes stage-matched embryo; +/+ denotes wild-type embryo; −/− denotes *Dnaaf2* mutant embryo. Posterior view, A; ventral view, B and C; lateral view, A′, B′ and C′; sagittal section of B, B′′.

well with the expression of *Dnaaf2* in mouse embryos (Fig. 1F). At E8.5, many apoptotic cells are already present in the embryonic portion of the mutants (Fig. 6A and B), also consistent with embryonic specific expression of *Dnaaf2* (Fig. 1). Appropriate growth and proliferation are essential for the embryo to advance. Turning of the embryo is an important process required for gut tube closure as well as the transition to fetal position for embryogenesis to proceed (37). The accumulation and increase in apoptotic cells may be a major reason for the early lethality of the *Dnaaf2*$^{-/-}$ embryos.

Discussion

Cilia are evolutionarily conserved cellular organelles that are found across a wide spectrum of species. Although once believed to be vestigial structures, it is now appreciated that most cells contain cilia and that cilia play critical roles in many signaling pathways and cellular functions (1–4,7). Research from the past decades has supported the essential role of cilia during normal embryogenesis (1,7). In humans, *DNAAF2* encodes a protein required for the preassembly of dynein arms, which is essential for cilia function and has been associated with diseases and disorders that are due to cilia defects (17,19,21). Here, for the first time we characterize the role of *Dnaaf2* during embryogenesis. Our data show that in the absence of *Dnaaf2* function, mouse embryos are delayed beginning at early gastrulation and do not progress past E9.5 stages.

Since cilia are essential for breaking left–right symmetry through of nodal flow, we carefully examined the nodes in mutant embryos. We show that the node is present morphologically and specified molecularly, although it is reduced in size with fewer cilia containing cells. We also show that although *Shh* expression is normal, left–right axis specification is disrupted in *Dnaaf2* mutant embryos.

Combined, these results suggest that the left–right defects present in *Dnaaf2* mutant embryos are due to a malfunction of cilia in the node. We speculate that the motility of these cilia is compromised due to dynein arm structural defects or malfunction in the absence of *Dnaaf2*, as suggested by previous reports in cell culture models (17,19). It is likely that the lack of *Dnaaf2* disrupts or weakens the leftward flow of the cilia at the node and which could result in the improper neural tube closure present in E9.5 *Dnaaf2* null embryos as cilia have also been implicated to play important roles in brain development (38–40). The embryonic yolk sac is one of the fetal membranes that contributes to the placenta (35). A previous large-scale mouse KO study shows a linkage between malformations in placental development and vascular, heart and brain defects in mid-gestation embryos (41). At E11.5, *Dnaaf2* mutant embryos display an obvious defect in yolk sac vasculature. Therefore, it is likely that yolk sac defects are present as early as E8.5, which may certainly contribute to the plethora of embryonic defects described above. It is also interesting that we observe an overall truncation phenotype in E9.5 *Dnaaf2*$^{-/-}$ embryos as past studies have shown that defects in cilia greatly affect planar cell polarity

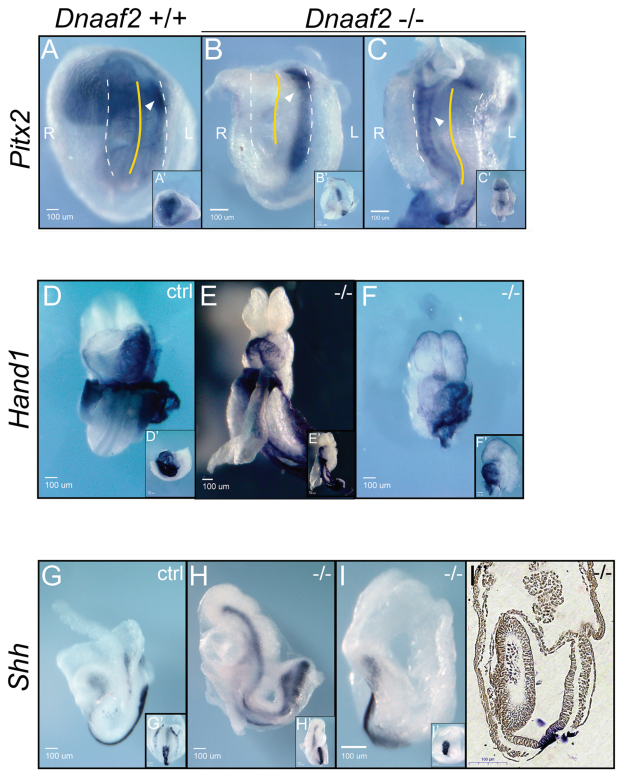

Figure 5. Left–right patterning gene expression in *Dnaaf2*$^{-/-}$ embryos. Embryos were collected at E8.5 (**A**, **B**, **G** and **I**) and E9.5 (**C**–**F** and **H**), and whole-mount ISH was performed with *Pitx2* (A–C), *Hand1* (D–F) or *Shh* (G–I) antisense probes. (A–C) *Pitx2*, a gene that is normally expressed in the left lateral plate mesoderm, is mis-expressed in the right lateral plate mesoderm in 25% of *Dnaaf2*$^{-/-}$ mutants. White triangles indicate Pitx2 expression; white dotted lines indicate the lateral-most sides of each embryo. Yellow dotted line shows midline of each embryo. R denotes the right side of the embryo, and L denotes the left side of the embryo. (D–F) *Hand1*, a gene that is expressed at the outer curvature of the left ventricle, is found on the opposite side in *Dnaaf2*$^{-/-}$ mutants. The looping of the heart is also reversed in the *Dnaaf2*$^{-/-}$ embryos. (G–I) *Shh* expression is not altered in the *Dnaaf2*$^{-/-}$ embryos. Both *Dnaaf2*$^{-/-}$ and wild-type embryos express *Shh* at the notochord. The white arrows refer to the expression of the indicated gene; ctrl denotes stage-matched embryo; –/–denotes *Dnaaf2* mutant embryo. Ventral view, A–C; lateral view, A′, G–I; frontal view, B′–C′ and D–F; lateral view, G′ and H′; ventral view, I′; sagittal sectioned of I, I′′.

signaling, which is essential for the convergence and extension movements during gastrulation (42,43).

As mentioned above, the knock-in reporter *LacZ* expression is narrowly expressed precisely in the node, a pattern that is quite different from *Dnaaf2* mRNA expression (compare Fig. 1C–G and Fig. 3D and E). We speculate that there must be enhancer or regulatory elements in the intronic sequence that direct wide-embryonic expression, and hence when a large portion of the *Dnaaf2* genomic sequence is removed, the node-specific reporter expression is the result. Further investigation of the promoter and intronic regions of the *Dnaaf2* locus may resolve this discrepancy and may elucidate a node-specific regulatory element, which may be of interest for future studies.

Intriguingly, when generated on an outbred ICR background, *Dnaaf2/Ktu* homozygous KO pups are found at birth, but 90% of these pups die prior to weaning (19). Importantly, similar to the phenotypes presented herein, these *Ktu* KO newborns exhibit *situs inversus totalis* and hydrocephaly (19). Importantly, we attempted to recapitulate this later phenotype by breeding the *Dnaaf2*$^{tm.1.1}$ onto an ICR background (data not shown). Although we did not recover newborn mutants at generation N5, homozygous mutant embryos displayed better developmental progress and could be recovered at later stages than C57bl/6NJ homozygotes. These data imply ICR-specific functional redundancy that compensates for *Dnaaf2* loss.

It is also curious that *Dnaaf4* and *Dnaaf5* are robustly expressed at slightly later stages than *Dnaaf2*. This raises the possibility that functional redundancy combined with subtle differences in the timing of expression of these genes may explain the variation observed in *Dnaaf2* phenotypes (lethal in C57bl/6NJ versus viable in ICR). Interestingly, *DNAAF2* loss of function in humans does not affect survival (17,44)—further indicating that *DNAAF* family member redundancies can compensate for the loss of the *DNAAF2* in humans but not C57bl/6NJ mice. It may therefore be of interest to map subtle differences between ICR and C57bl/6NJ embryonic *Dnaaf* expression patterns as well as to explore patterns of *Dnaaf* in other mammalian species.

Materials and Methods

Animals

The Dnaaf2 KO allele was generated by the Jackson Laboratory (stock no. 024570: *Dnaaf2*$^{tm1.1(KOMP)Vlcg}$). In brief, 8457 bp of the *Dnaaf2* genomic sequence was replaced with the *lacZ* reporter in C57BL/6NJ mouse embryonic stem cells removing part of exon 1, intron 1 and exon 2, intron 2 and part of exon 3 (Fig. 3C).

Embryo retrieval and genotyping

Dnaaf2 $^{-/-}$ embryos were generated by heterozygote intercosses. Males and females were housed together, and the presence of the vaginal plugs was defined as E0.5. Genotypes of individual embryos were determined by PCR using primers (given 5′ to 3′): wild type (ATCTAAGCCCCGTCGGTTAC and ACCGTGAAGGC TTAAGAGCA) and KO (CGGTCGCTACCATTACCAGT and TAGC TAGGCATTGGGATTGC). Specific genotyping protocol is available at https://www.jax.org/strain/024570 (stock no. 024570). All results shown were repeated on a minimum of three mutant embryos except for E11.5 and E13.5 embryos shown in Figure 2. Use of animals was approved by the University of Massachusetts Institutional Animal Care and Use Committee (IACUC).

RNA extraction and RT-PCR analysis

RNA was extracted using Roche High Pure RNA Isolation Kit (Roche Diagnostics, Indianapolis, Indiana USA, 11828665001). cDNA synthesis was performed using Bio-Rad iScript cDNA Synthesis (Bio-Rad, Hercules, California USA, 1708890). RT-PCR was performed for 35 cycles of 30 s at 60°C, 72°C and 95°C with the following primers with indicated gene names unless otherwise specified (given 5′ to 3′): *Dnaaf1* (359 bp): GCCTCTTCCTGCAAGT GAAC and GTGCTTCAGACGGACAGTGA; *Dnaaf2* (583 bp): TCTGC CACAAACTCTTCACG and GCCCAGCAGGATCACTACAT; *Dnaaf3* (301 bp): GGCACCGGTTATGGTAGTGT and CTTGGAGCCCCATCTT CTC; *Dnaaf4* (319 bp): AAACTATTTGGCAGCGGTTG and CCGAATC TTCTCTGCATCGT; *Dnaaf5* (348 bp): CCTCAAGAATTCAGGGGACA and AGCTGCTCGCAGTAGGTAGC; *T* (313 bp): CATGTACTCTTTCT TGCTGG and GGTCTCGGGAAAGCAGTGGC; *Gapdh* (452 bp): ACCACAGTCCATGCCATCAC and TCCACCACCCTGTTGCTGTA.

RT-PCR analyses for E6.5 C57BL/6NJ and ICR mouse embryos in Figure 2 were performed under the following condition: 33 cycles of 30 s at 60°C, 72°C and 95°C.

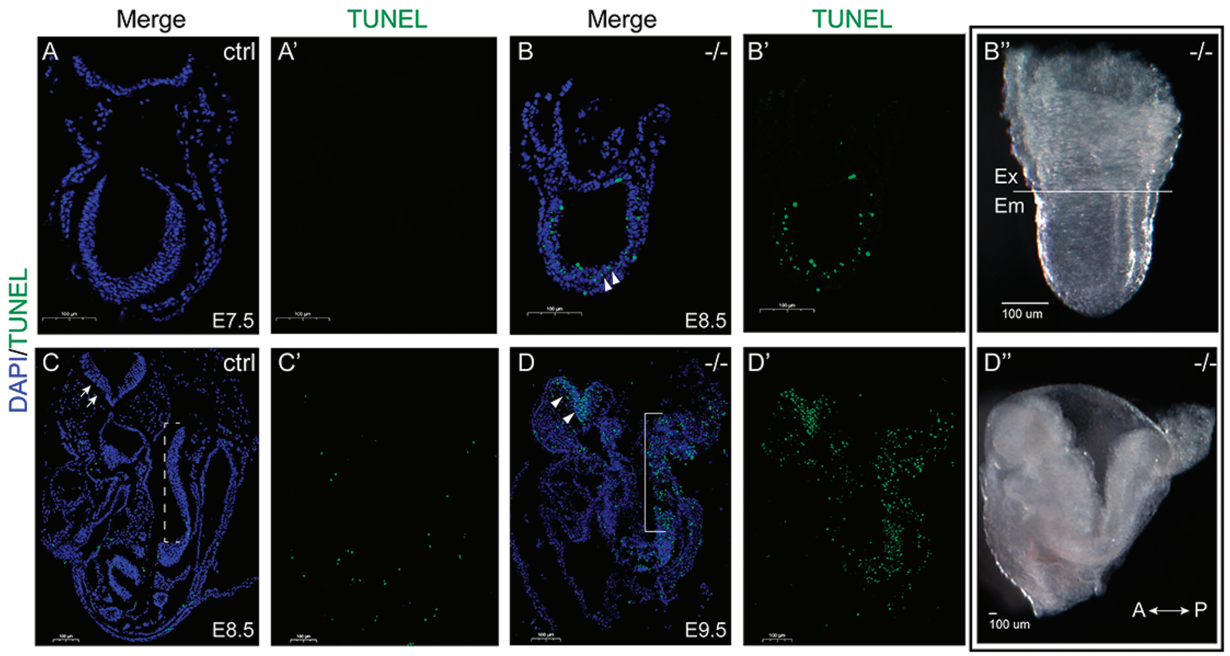

Figure 6. TUNEL assay in *Dnaaf2*$^{-/-}$ embryos and their stage-matched control embryos (**A** and **B**; **C** and **D**). Embryos were collected at the indicated embryonic day (A–D) and processed for TUNEL assay. (A–D) Compared to stage-matched control embryos, E8.5 *Dnaaf2*$^{-/-}$ embryo displays apoptotic cells in the embryonic portion (white triangles in B). At E9.5, TUNEL-positive cells accumulate at the neural tube (white triangles in D) and the tail region of the *Dnaaf2*$^{-/-}$ embryos (white triangles and bracket in D), whereas the stage-matched control embryo experience minimal apoptosis (white arrows and dotted bracket in C). B'' and D'' are whole-mount images of embryos sectioned for B and D. Sagittal sectioned, A–D. Ex denotes extraembryonic portion; em denotes embryonic portion; A denotes anterior axis; P denotes posterior axis; ctrl denotes stage-matched embryo; –/– denotes *Dnaaf2* mutant embryo.

Whole-mount ISH

Freshly dissected embryos were fixed in 4% paraformaldehyde for 2–4 h on ice and subjected to modification from Tremblay *et al.* (2001) (45). Embryos were then dehydrated in methanol and stored up to 1 month. Embryos were rehydrated in a series of methanol in 1× PBT. Subsequently, the embryos were rinsed in 1× PBT for 5 min twice and bleached in 6% hydrogen peroxide for 1 h. Embryos were then rinsed with 1× PBT, proceeded with proteinase K treatment for 6–8 min and incubated with glycine in 1× PBT for 5 min. After rinsing with 1× PBT for 5 min twice, embryos were fixed with 4% paraformaldehyde with 0.02% glutaraldehyde for 20 min. Embryos were rinsed in 1× PBT for 5 min twice and incubated in 1:1 hybridization buffer/PBT for 10 min and subsequently in hybridization buffer for 10 min. The embryos were then incubated with 150 ng RNA probes in hybridization buffer at 70°C overnight. The next day, embryos were washed with solutions containing formamide, 20× SSC, 1 M citric acid, 20% SDS and Tween 20 for 30 min at 70°C for the first 3 washes and at 65°C for the last 3 washes. Following this, the embryos were rinsed in 1× maleic acid buffer containing levamisole for 5 min 3 times. The embryos were then blocked in maleic acid buffer with 2% Boehringer blocking reagent for 1 h at room temperature and then incubated with the antibody solution containing Anti-Digoxigenin-AP (Roche Diagnostics, Indianapolis, Indiana USA, 11093274910), heat activated sheep serum (Sigma-Aldrich, St. Louis, Missouri USA, S2263) and levamisole (Sigma-Aldrich, St. Louis, Missouri USA, L9756) at 4°C overnight. The following day, the embryos were washed with 1× maleic acid buffer containing levamisole for at least 1 h 6 times. The embryos were then rinsed with alkaline phosphatase buffer containing 1 M Tris-HCl pH 9.5, 5 M NaCl, 1 M $MgCl_2$ and Tween 20 for 10 min 3 times and developed in BM purple solution (Roche Diagnostics, Indianapolis, Indiana USA, 11442074001) until the color has developed. The embryos were then washed with 1× PBT containing 0.5 M EDTA, fixed in 4% paraformaldehyde overnight, dehydrated in a series of ethanol, cleared in xylene, embedded with paraffin and sectioned at 7 um thick. Antisense probes were generated using E7.5 embryonic cDNA. RT-PCR was performed for 35 cycles of 30 s at 60°C, 72°C and 95°C with the following primers with indicated genes. The amplicons were then cloned into the TOPO TA Cloning Vectors using the TOPO TA Cloning kit for Sequencing (Invitrogen, Waltham, Massachusetts USA, 450030) according to the manufacturer's instructions.

Probes used were the following: *Cthrc1* (554 bp): TGCTGC TGCTACAGTTGTCC and CCCTTCACAGAGTCCTTCCA; *Dnaaf2* (intron-spanning primers designed to generate an amplicon that includes exon 1 to exon 3; 583 bp): TCTGCCACAAACTCTTCACG and GCCCAGCAGGATCACTACAT; *Hand1* (574 bp): CCATCATCAC CACTCACACC and GCGCCCTTTAATCCTCTTCT; *Pitx2* (46); and *Shh* (47).

X-gal (5-bromo-4-chloro-3-indolyl-β-D-galactopyranoside) staining

Freshly dissected embryos were fixed in X-gal buffer containing 0.2% glutaraldehyde and 1% formaldehyde on ice for 15 min and subjected to modification from Tremblay *et al.* (2000) (48). In brief, the fixed embryos were washed with X-gal buffer (PBS, 5 mM EGTA, 2 mM MgCl:$6H_2O$, 0.2% NP-40, 0.2 mM deoxycholate) for 10 min 3 times and stained with X-gal stain (X-gal buffer, 5 mM potassium ferricyanide and 5 mM potassium ferrocyanide and 0.5 mg/ml X-gal) overnight at 37°C. Subsequently, embryos were dehydrated in ethanol, cleared in xylene, embedded with paraffin and sectioned at 7 um thick. The sectioned embryos

were deparaffinated and rehydrated for subsequent processing. Eosin staining was performed by immersing rehydrated sectioned embryos in eosin Y solution for 15–20 s, followed by 95% ethanol for 2 min and then 100% ethanol for 2 min and lastly cleared in xylene. Slides were then sealed with Cytoseal 60. X-gal stained sections were imaged with a Panoramic MIDI II slide scanner (3DHISTECH, Budapest, Hungary).

Immunofluorescence

Freshly dissected embryos were fixed in 4% paraformaldehyde overnight, dehydrated in ethanol, cleared in xylene, embedded with paraffin and sectioned at 7 um thick. The sectioned embryos were deparaffinated and rehydrated for subsequent procedures. Antigen retrieval was performed by boiling in 0.01 M Tris-Base pH 10 with 0.05% Tween 20 for 4 min and allowed to cool to room temperature. The slides were then rinsed with 1× PBT for 2 min twice. Primary antibodies were incubated at 4°C overnight in a humid chamber. The slides were then rinsed with 1× PBT for 15 min 3 times, followed by incubation with secondary antibodies at room temperature for 1 h in a humid chamber. Subsequently, the slides were rinsed with 1× PBS for 15 min 3 times. Nuclei were counterstained with (DAPI) in PBS (1:10000) for 3 min. Slides were rinsed with 1× PBS and sealed with ProLong Gold. Immunofluorescence slides were imaged with Panoramic MIDI II slide scanner (3DHISTECH).

Primary antibodies were used in the following conditions: T (Santa Cruz Biotechnology, Inc, Dallas, Texas USA; 1:100); Ecad (Abcam, Cambridge, Massachusetts USA; 1:1000); and Arl13b (Proteintech, Rosemont, Illinois USA; 17711-1-AP, 1:250). Secondary antibodies were used in the following conditions: Alexa fluor 488 donkey anti-mouse (Thermo Fisher Scientific, Waltham Massachusetts USA; A-21202, 1:500); 647 donkey anti-goat (Thermo Fisher Scientific, Waltham Massachusetts USA; A-21447, 1:500); and 546 donkey anti-rabbit (Thermo Fisher Scientific, Waltham Massachusetts USA; A10040, 1:500). DAPI concentration (Molecular Probes, Waltham, Massachusetts USA; 1:10000).

Assessment of apoptosis

Apoptosis was assessed using *In Situ* Cell Death Detection Kit (Roche Diagnostics, Indianapolis, Indiana USA, 11684795910). Freshly dissected embryos were fixed in 4% paraformaldehyde overnight, dehydrated in ethanol, cleared in xylene, embedded with paraffin and sectioned at 7 um thick. The sectioned embryos were deparaffinated and rehydrated for the TUNEL technology according to manufacturer's protocol.

Imaging

Digital images of whole-mount embryos were captured on a Nikon SMZ-1500 stereomicroscope equipped with a Spot Idea Digital Camera and Spot software (v4.6). Images of sectioned embryos were taken with a Pannoramic MIDI slide scanner or Nikon Eclipse 50i equipped with a Spot Idea Digital Camera and Spot software (v4.6) or Nikon Eclipse Ti inverted microscope with an Andor DR-228C camera and Nikon NIS Elements AR software.

Acknowledgements

We would like to thank members of the Mager and Tremblay laboratories for providing useful input throughout the project.

Conflict of Interest statement. None declared.

Funding

Funded in part by National Institutes of Health (R01HD083311 to J.M.).

References

1. Sung, C.H. and Leroux, M.R. (2013) The roles of evolutionarily conserved functional modules in cilia-related trafficking. *Nat. Cell Biol.*, **15**, 1387–1397.
2. Veland, I.R., Awan, A., Pedersen, L.B., Yoder, B.K. and Christensen, S.T. (2009) Primary cilia and signaling pathways in mammalian development, health and disease. *Nephron Physiol.*, **111**, 39–53.
3. Goetz, S.C. and Anderson, K.V. (2010) The primary cilium: a signalling centre during vertebrate development. *Nat. Rev. Genet.*, **11**, 331–344.
4. Basten, S.G. and Giles, R.H. (2013) Functional aspects of primary cilia in signaling, cell cycle and tumorigenesis. *Cilia*, **2**, 1–23.
5. Pazour, G.J. and Witman, G.B. (2003) The vertebrate primary cilium is a sensory organelle. *Curr. Opin. Cell Biol.*, **15**, 105–110.
6. Shah, A.S., Ben-Shahar, Y., Moninger, T.O., Kline, J.N. and Welsh, M.J. (2009) Motile cilia of human airway epithelia are chemosensory. *Science*, **325**, 1131–1134.
7. Drummond, I.A. (2012) Cilia functions in development. *Curr. Opin. Cell Biol.*, **24**, 24–30.
8. Downs, K.M. (2009) The enigmatic primitive streak: prevailing notions and challenges concerning the body axis of mammals. *Bioessays*, **31**, 892–902.
9. Supp, D.M., Witte, D.P., Potter, S.S. and Brueckner, M. (1997) Mutation of an axonemal dynein affects left–right asymmetry in inversus viscerum mice. *Nature*, **389**, 963–966.
10. Pennekamp, P., Menchen, T., Dworniczak, B. and Hamada, H. (2015) Situs inversus and ciliary abnormalities: 20 years later, what is the connection? *Cilia*, **4**, 1–12.
11. Levin, M. (2004) Left–right asymmetry in embryonic development: a comprehensive review. *Mech. Dev.*, **122**, 3–25.
12. Shiratori, H. and Hamada, H. (2006) The left–right axis in the mouse: from origin to morphology. *Development*, **133**, 2095–2104.
13. Brennan, J., Norris, D.P. and Robertson, E.J. (2002) Nodal activity in the node governs left–right asymmetry. *Genes Dev.*, **16**, 2339–2344.
14. Tsukui, T., Capdevila, J., Tamura, K., Ruiz-Lozano, P., Rodriguez-Esteban, C., Yonei-Tamura, S., Magallón, J., Chandraratna, R.A., Chien, K., Blumberg, B. *et al.* (1999) Multiple left–right asymmetry defects in Shh(−/−) mutant mice unveil a convergence of the Shh and retinoic acid pathways in the control of Lefty-1. *Proc. Natl. Acad. Sci. U. S. A.*, **96**, 11376–11381.
15. Nonaka, S., Tanaka, Y., Okada, Y., Takeda, S., Harada, A., Kanai, Y., Kido, M. and Hirokawa, N. (1998) Randomization of left–right asymmetry due to loss of nodal cilia generating leftward flow of extraembryonic fluid in mice lacking KIF3B motor protein. *Cell*, **95**, 829–837.
16. Supp, D.M., Brueckner, M., Kuehn, M.R., Witte, D.P., Lowe, L.A., McGrath, J., Corrales, J. and Potter, S.S. (1999) Targeted deletion of the ATP binding domain of left–right dynein confirms its role in specifying development of left–right asymmetries. *Development*, **126**, 5495–5504.
17. Omran, H., Kobayashi, D., Olbrich, H., Tsukahara, T., Loges, N.T., Hagiwara, H., Qi, Z., Leblond, G., O'Toole, E., Hara, C. *et al.* (2008) Ktu/PF13 is required for cytoplasmic pre-assembly of axonemal dyneins. *Nature*, **456**, 611–616.

18. Mitchison, H.M., Schmidts, M., Loges, N.T., Freshour, J., Dritsoula, A., Hirst, R.A., O'Callaghan, C., Blau, H., Al, M., Olbrich, H. *et al.* (2012) Mutations in axonemal dynein assembly factor DNAAF3 cause primary ciliary dyskinesia. *Nat. Genet.*, **44**, 381–389.
19. Matsuo, M., Shimada, A., Koshida, S., Saga, Y. and Takeda, H. (2013) The establishment of rotational polarity in the airway and ependymal cilia: analysis with a novel cilium motility mutant mouse. *Am. J. Physiol. Lung Cell. Mol. Physiol.*, **304**, L736–L745.
20. Tarkar, A., Loges, N.T., Slagle, C.E., Francis, R., Dougherty, G.W., Tamayo, J.V., Shook, B., Cantino, M., Schwartz, D., Jahnke, C. *et al.* (2013) DYX1C1 is required for axonemal dynein assembly and ciliary motility. *Nat. Genet.*, **45**, 995–1003.
21. Raidt, J., Wallmeier, J., Hjeij, R., Onnebrink, J.G., Pennekamp, P., Loges, N.T., Olbrich, H., Häffner, K., Dougherty, G.W., Omran, H. *et al.* (2014) Ciliary beat pattern and frequency in genetic variants of primary ciliary dyskinesia. *Eur. Respir. J.*, **44**, 1579–1588.
22. Afzelius, B. (2004) Cilia-related diseases. *J. Pathol.*, **204**, 470–477.
23. Brown, J.M. and Witman, G.B. (2014) Cilia and diseases. *Bioscience*, **64**, 1126–1137.
24. Zihlif, N., Paraskakis, E., Tripoli, C., Lex, C. and Bush, A. (2006) Markers of airway inflammation in primary ciliary dyskinesia studied using exhaled breath condensate. *Pediatr. Pulmonol.*, **41**, 509–514.
25. Maimoona, A., Zariwala, M.R.K. and Omran, H. (2007) Genetic defects in ciliary structure and function. *Annu. Rev. Physiol.*, **69**, 423–450.
26. Dickinson, M.E., Flenniken, A.M., Ji, X., Teboul, L., Wong, M.D., White, J.K., Meehan, T.F., Weninger, W.J., Westerberg, H., Adissu, H. *et al.* (2016) High-throughput discovery of novel developmental phenotypes. *Nature*, **537**, 508–514.
27. Ayadi, A., Birling, M.C., Bottomley, J., Bussell, J., Fuchs, H., Fray, M., Gailus-Durner, V., Greenaway, S., Houghton, R., Karp, N. *et al.* (2012) Mouse large-scale phenotyping initiatives: overview of the European Mouse Disease Clinic (EUMODIC) and of the Wellcome Trust Sanger Institute Mouse Genetics Project. *Mamm. Genome*, **23**, 600–610.
28. Miao, C., Jiang, Q., Li, H., Zhang, Q., Bai, B., Bao, Y. and Zhang, T. (2016) Mutations in the motile cilia gene DNAAF1 are associated with neural tube defects in humans. *G3 (Bethesda)*, **6**, 3307–3316.
29. Horani, A., Ustione, A., Huang, T., Firth, A.L., Pan, J., Gunsten, S.P., Haspel, J.A., Piston, D.W. and Brody, S.L. (2018) Establishment of the early cilia preassembly protein complex during motile ciliogenesis. *Proc. Natl. Acad. Sci. U. S. A.*, **115**, 1221–1228.
30. Diggle, C.P., Moore, D.J., Mali, G., zur Lage, P., Ait-Lounis, A., Schmidts, M., Shoemark, A., Munoz, A.G., Halachev, M.R., Gautier, P. *et al.* (2014) HEATR2 plays a conserved role in assembly of the ciliary motile apparatus. *PLoS Genet.*, **10**, 1–20.
31. Lyons, R.A., Saridogan, E. and Djahanbakhch, O. (2006) The reproductive significance of human fallopian tube cilia. *Hum. Reprod. Update*, **12**, 363–372.
32. Ou, Y., Dores, C., Rodriguez-Sosa, J.-R., van der Hoorn, F.A. and Dobrinski, I. (2014) Primary cilia in the developing pig testis. *Cell Tissue Res.*, **358**, 597–605.
33. Dores, C., Alpaugh, W., Lin, S., Biernaskie, J. and Dobrinski, I. (2017) Primary cilia on porcine testicular somatic cells and their role in hedgehog signaling and tubular morphogenesis in vitro. *Cell Tissue Res.*, **368**, 215–223.
34. Garcia, M.D. and Larina, I.V. (2014) Vascular development and hemodynamic force in the mouse yolk sac. *Front. Physiol.*, **5**, 1–10.
35. Freyer, C. and Renfree, M.B. (2009) The mammalian yolk sac placenta. *J. Exp. Zool. B Mol. Dev. Evol.*, **312**, 545–554.
36. Yamamoto, S., Nishimura, O., Misaki, K., Nishita, M., Minami, Y., Yonemura, S., Tarui, H. and Sasaki, H. (2008) Cthrc1 selectively activates the planar cell polarity pathway of Wnt signaling by stabilizing the Wnt-receptor complex. *Dev. Cell*, **15**, 23–36.
37. Spence, J.R., Lauf, R. and Shroyer, N.F. (2011) Vertebrate intestinal endoderm development. *Dev. Dyn.*, **240**, 501–520.
38. Han, Y.G. and Alvarez-Buylla, Y. (2010) Role of primary cilia in brain development and cancer. *Curr. Opin. Neurobiol.*, **20**, 58–67.
39. Faubel, R., Westendorf, C., Bodenschatz, E. and Eichele, G. (2016) Cilia-based flow network in the brain ventricles. *Science*, **353**, 176–178.
40. Foerster, P., Daclin, M., Asm, S., Faucourt, M., Boletta, A., Genovesio, A. and Spassky, N. (2017) mTORC1 signaling and primary cilia are required for brain ventricle morphogenesis. *Development*, **144**, 201–210.
41. Perez-Garcia, V., Fineberg, E., Wilson, R., Murray, A., Mazzeo, C.I., Tudor, C., Sienerth, A., White, J.K., Tuck, E., Ryder, E.J. *et al.* (2018) Placentation defects are highly prevalent in embryonic lethal mouse mutants. *Nature*, **555**, 463–468.
42. Ross, A.J., May-Simera, H., Eichers, E.R., Kai, M., Hill, J., Jagger, D.J., Leitch, C.C., Paul Chapple, J., Munro, P.M., Fisher, S. *et al.* (2005) Disruption of Bardet–Biedl syndrome ciliary proteins perturbs planar cell polarity in vertebrates. *Nat. Genet.*, **37**, 1135–1140.
43. Wallingford, J.B. (2006) Planar cell polarity, ciliogenesis and neural tube defects. *Hum. Mol. Genet.*, **15**, R227–R234.
44. Lek, M., Karczewski, K.J., Minikel, E.V., Samocha, K.E., Banks, E., Fennell, T., O'Donnell-Luria, A.H., Ware, J.S., Hill, A.J., Cummings, B.B. *et al.* (2016) Analysis of protein-coding genetic variation in 60,706 humans. *Nature*, **536**, 285–291.
45. Tremblay, K.D., Dunn, N.R. and Robertson, E.J. (2001) Mouse embryos lacking Smad1 signals display defects in extraembryonic tissues and germ cell formation. *Development*, **128** 3609–3621.
46. Ryan, A.K., Blumberg, B., Rodriguez-Esteban, C., Yonei-Tamura, S., Tamura, K., Tsukui, T., de la Peña, J., Sabbagh, W., Greenwald, J., Choe, S. *et al.* (1998) Pitx2 determines left–right asymmetry of internal organs in vertebrates. *Nature*, **394**, 545–551.
47. Echelard, Y., Epstein, D.J., St-Jacques, B., Shen, L., Mohler, J., McMahon, J.A. and McMahon, A.P. (1993) Sonic hedgehog, a member of a family of putative signaling molecules, is implicated in the regulation of CNS polarity. *Cell*, **75**, 1417–1430.
48. Tremblay, K.D., Hoodless, P.A., Bikoff, E.K. and Robertson, E.J. (2000) Formation of the definitive endoderm in mouse is a Smad2-dependent process. *Development*, **127**, 3079–3090.